Mater. Res. Soc. Symp. Proc. Vol. 1454 © 2012 Materials Research Society
DOI: 10.1557/opl.2012.1129

Electrical Transport in Ultrathin $NdNiO_3$ Films

Megan Campbell and Ashutosh Tiwari*
Nanostructured Materials Research Laboratory
University of Utah, Department of Materials Science & Engineering
*E-mail: tiwari@eng.utah.edu

ABSTRACT

Electrical transport properties in ultrathin $NdNiO_3$ films grown on single crystal $LaAlO_3$ (001) substrate were characterized. Films with thicknesses ranging from 0.6 nm to 12 nm were grown using a pulsed laser technique. Four probe resistivity as a function of temperature measurements indicated a strong dissipation of strain effects from 0.6 nm to 6 nm as well as the presence of defects in the 12 nm sample. A proposed mechanism of kinetically stable glassy phase formation explains the time dependence of the resistivity in both cooling and heating cycles.

INTRODUCTION

Electrical transport in strongly correlated transition metal oxides has been a subject of great scientific interest over the last several decades. Many interesting properties such as, high temperature superconductivity [1, 2], colossal magnetoresistance [3, 4] and multi-ferroelectricity [5, 6] have been observed in these systems. Typical examples of such materials are perovskite oxides like YBCO, LSMO, $YMnO_3$ and $BiFeO_3$. $NdNiO_3$ is another very interesting, but less well understood, member of this family [7]. It possesses orthorhombic perovskite structure and behaves as a metal at high temperatures, as an insulator at low temperatures and undergoes a metal-insulator (M-I) transition in the intermediate temperature range. The M-I transition in $NdNiO_3$ is understood to arise due to the closing of charge-transfer gap between the oxygen 2p and Ni 3d upper Hubbard band. Specifically, in the low temperature phase, the Fermi level lies in the charge transfer gap resulting in an insulating behavior. However, as the temperature is increased, the energy bands get broadened and at the M-I transition temperature, T_{M-I}, they start overlapping, resulting in a metallic phase.

The crystallographic unit cell of perovskite oxides (ABO_3) comprises of corner sharing BO_6 octahedra forming a three dimensional network. In the case of cubic perovskites, BO_6 octahedra are arranged regularly at the nodes of a simple cubic lattice forming B-O-B bond angles of 180^0 (Figure 1 (a)) [8]. In the case of orthorhombic perovskites such as $NdNiO_3$, NiO_6 octahedra are tilted and Ni-O-Ni angles are less than 180^0 (Figure 1 (b)). On decreasing the size of atom A in orthorhombic perovskites, the B-O-B angles can be much lower than 180^0. Based on neutron diffraction experiments, it has been demonstrated that the charge-transfer M-I transition in $NdNiO_3$ is related to changes in the Ni-O-Ni bond angle [9]. The more the BO_6 octahedra are able to rotate in orthorhombic perovskites, the higher the T_{M-I}. [10]

When external pressure is applied, the Ni-O-Ni bond angles straighten and T_{M-I} decreases [11, 12]. Obradors *et al.* [13] showed that on applying external hydrostatic pressure, the T_{M-I} in $NdNiO_3$ can be decreased with a rate $dT_{M-I}/dP = -4.8$ K/kbar. In another study on thin films, Tiwari *et al.* showed that T_{M-I} can be both decreased and increased. Specifically they showed that films under tensile stress (i.e. films grown on $SrTiO_3$ substrate) show a decrease in T_{M-I} while the

films under compressive stress (i.e. films grown on $LaAlO_3$ substrate) show an increase in T_{M-I}. They demonstrated that by varying stress in $NdNiO_3$ films, T_{M-I} can be tuned over the range 300 K to 10K [14].

Though the work reported by Tiwari *et al* is very important from the point of making room-temperature sensors and devices, their $NdNiO_3$ films were grown on Si (100) substrates with intermediate buffer layers [14]. Moreover, the thicknesses of the films were several in the range 10 nm-30 nm. In that situation, other effects may also be playing role in addition to epitaxial stress. Epitaxial stress effects are more dominant when films are very thin and are grown on single crystal substrates. So, in order to procure a better understanding of the effect of stress on the M-I transition of $NdNiO_3$, here we are reporting the electrical transport properties of ultrathin (0.6 nm- 12 nm) $NdNiO_3$ films grown directly on single crystal $LaAlO_3$ substrate.

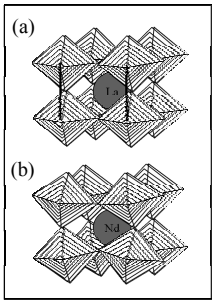

Figure 1. Structure of: (a) Cubic perovskite $LaNiO_3$ and (b) Orthorhombic perovskite $NdNiO_3$.

EXPERIMENT

Thin films of $NdNiO_3$ were grown by pulsed laser deposition with a KrF excimer laser (λ = 248 nm and pulse width of 25 ns) from a ceramic target onto the single crystal $LaAlO_3$ (001). The growth occurred under 0.3 mbar O_2, at a substrate temperature of 700^0C, with the laser energy density of ~15 J/cm^2, a substrate-to-target distance of 4.5 cm, and 10 Hz pulse frequency. Following the deposition, the samples were annealed in 0.5 mbar O_2 for 30 minutes. Depositions of 25 – 500 pulses yielded films ranging from 0.6 – 12 nm thick. Using a test sample, a Tencor P-10 profilometer was used to verify the deposition rate and thus film thickness.

Using a Phillips X-PERT X-ray Diffractometer which employs Cu Kα radiation, X-ray diffraction was performed on the samples to examine lattice changes due to film thickness. A conventional four-probe technique was used to examine the resistance of the samples, utilizing a Keithley 6220 current source and a Keithley 181 nanovoltmeter. In order to investigate the temperature dependence, a closed cycle cryostat (CTI cryogenics Model 22) was used to attain a temperature range of 17 – 300 K. A Lakeshore temperature controller moderated the temperature in these measurements and a ramp rate of 10 K/min was used.

RESULTS AND DISCUSSION

X-ray Crystallography

$NdNiO_3$ films grown on $LaAlO_3$ showed good crystallinity over the range of thicknesses deposited (Figure 2). Due to the resolution of the X-ray diffractometer, it was impossible to distinguish the $LaAlO_3$ substrate peaks from the $NdNiO_3$ film peaks. The peaks located at approximately 23^0 2θ and 47^0 2θ can be attributed to either the {110} pseudo-cubic orientation, or the {200} orthorhombic orientation with previous research indicating a higher probability for the orthorhombic orientation of lattice symmetry *Pbnm* [15, 16]. The bulk pseudo-cubic lattice constant of $LaAlO_3$ is 3.790 Å and 3.818 Å for bulk $NdNiO_3$, resulting in small compressive strain acting on the $NdNiO_3$ thin film, which is oriented with its pseudo-cubic axes parallel to those of the $LaAlO_3$. The presence of epitaxial growth has been supported by the work performed by Liu *et al* [17].

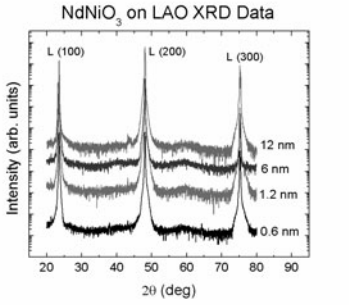

Figure 2. XRD data for $NdNiO_3$ deposited on $LaAlO_3$. No significant differences could be seen by examining the scans for the varying thicknesses.

Electrical Resistance

The resistivity vs. temperature is shown in Figure 3. For films of approximately 0.6 nm thick, the resistivity values and T_{M-I} were much higher than for other samples. Based on the pseudo-cubic lattice of $NdNiO_3$ thin films, a thickness of 0.6 nm is equivalent to approximately two unit cells thick. The atoms of $NdNiO_3$ are constrained to the substrate lattice. This constriction leads to a compressive stress acting on the $NdNiO_3$ atoms [18] and a subsequent decrease in the Ni-O-Ni angle. The 0.6 nm thick film is held in a more rigid structure than thicker films, causing it to exhibit more insulative behavior, indicated by its resistivity as well as its T_{M-I}, which was not observed below room temperature.

Likewise, 1.2 nm thick films also exhibit highly insulative behavior. However, the T_{M-I} occurs at a much lower temperature, near 170 K. This indicates that, although still limited in the freedom of its motion, the 1.2 nm thick $NdNiO_3$ is under much less strain than the 0.6 nm thick sample. This rapid dissipation of the strain effects is also seen in the 6 nm thick sample. Still containing a sharp transition, the 6 nm thick sample has a T_{M-I} between 160 and 185 K.

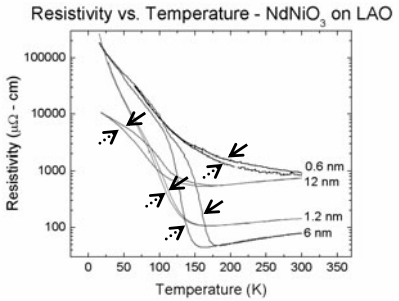

Figure 3. Resistivity vs. temperature for 17 – 300 K. The cooling cycle is indicated by the dashed arrow, the lower curve in each case, and the heating cycle is indicated by the solid arrow, upper curve, for each of the samples.

Following a similar trend, the 12 nm thick sample exhibited a transition between 165 and 175 K. However, this sample also exhibited a significant difference in the behavior of its resistivity, which can be explained by the $NdNiO_3$ film growth. As the thickness was increased to 12 nm, the structure changed from that of strained defect free film growth to a strain film with significant defects present. The presence of these defects impeded the motion of the electrons, acting like scattering centers, causing the sample to exhibit relatively high resistivity values.

The dependence of resistivity on film thickness was directly related to the temperature at which the resistivity was measured. At 17 K, as shown in Figure 4, the resistivity of the 1.2 nm thick film was higher than the resistivity of the 6 nm thick film, as was to be expected for the lessened strain associated with the increased film thickness. However, for 12 nm thick, the resistivity was much lower than anticipated, occurring well below the resistivity values of smaller thicknesses. We suggest that, at low temperatures, the strain effects dominate over defects for epitaxial films. As the strain for the 12 nm thick sample is minimal, the resistivity is likewise minimized. At the T_{M-I} and 300K, the resistivity for the 1.2 and 6 nm thick films followed the same trend as when at 17 K, decreasing as the film thickness increased (Figure 5). An increase in resistivity was observed for the 12 nm thick sample, consistent with the idea that at and above the T_{M-I}, the strain effects on the resistivity are dominated by defect effects.

The presence of hysteresis on the resistivity vs. temperature plots was a direct result of structural changes in the $NdNiO_3$ and indicated a time dependence of the cycle. Thus, the resistivity of the 1.2, 6, and 12 nm samples was also measured as a function of time in Figure 6. For the cooling cycle, the samples were cooled to the temperature at which the maximum hysteresis occurred, where the resistivity was measured over time. For the 1.2 nm thick sample, the resistivity showed little change with time, increasing by only about one percent. However, as the thickness was increased to 6 nm, the resistivity enlarged by approximately thirteen percent. Finally, increasing to 12 nm, the resistivity experienced a moderate change of around eight percent.

For the heating cycle, similar data were taken (see Figure 7). As can be seen with the 1.2 nm thick sample, the change in the resistivity varied by almost eight percent. The 6 nm thick sample

resistivity changed similarly with time, exhibiting a change of around 15 percent. The resistivity vs. time data for the 12 nm sample showed a change in resistivity that is around one percent.

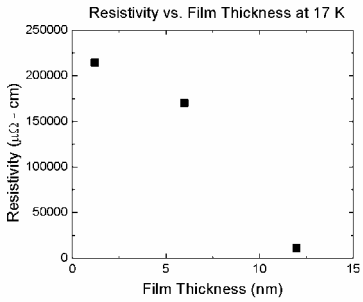

Figure 4. Resistivity vs. film thickness at 17 K. The 0.6 nm sample is not shown, as its resistivity was too high to measure at 17 K.

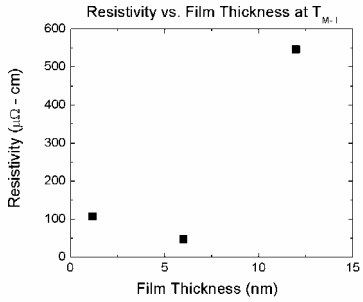

Figure 5. Resistivity vs. film thickness at T_{M-I}. The same trend was seen at 300 K. Again, the 0.6 nm sample is not shown because a T_{M-I} was never reached.

Based on this time dependent data, the structural behavior of $NdNiO_3$ at low temperatures can be inferred. It is proposed that the 1.2 nm sample transitions to a kinetically arrested glassy state, with little supercooling [19, 20]. As the temperature was decreased, the metallic state supercooled slightly, with most of this state directly forming the glassy state.

This behavior gave rise to the low resistivity change seen in the 1.2 nm sample on cooling. However, on heating, the return of the glassy state to the supercooled metallic state led to time dependence. In the case of the 6 nm sample, the degree of supercooling was high, showing similar time dependence for the heating and cooling cycles. For the 12 nm sample, the sample again showed a high degree of supercooling, with less glassy phase than the other samples. This is consistent with the proposed structure of a defect ridden 12 nm sample, as those defects help prevent the formation of large phases of glassy state.

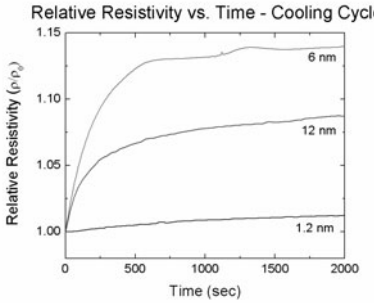

Figure 6. Cooling cycle resistivity vs. time.

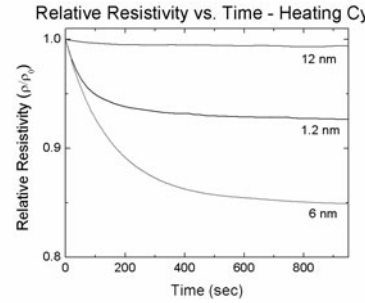

Figure 7. Heating cycle resistivity vs. time.

CONCLUSIONS

Based on the X-ray crystallography and resistivity measurements, a proposed structure of strain effects and compensating defects is consistent. For the thinnest sample, the strain was maximized, resulting in a Ni-O-Ni bond angle much smaller than 180^0. Thus the resistivity and the T_{M-I} were likewise maximized. Further, for the 1.2 nm sample, the strain was relatively less, by still defect free and constrained to the substrate lattice. Similarly for 6 nm of $NdNiO_3$, the resistivity was decreased, as the strain reached a minimum. The presence of defects in the 12 nm sample resulted in a strongly disordered structure with similar behavior to the bulk data. Using a model of a supercooled metallic state transitioning to a kinetically stable glassy state, the physical change associated with the M-I transition can likewise be understood.

REFERENCES

1. J. G. Bednorz and K. A. Müller, *Z. Phys. B. – Condens. Matter* **64**, 2 (1986).
2. A. Bussmann-Holder, A. Simon, and H. Buttner, *Phys. Rev. B.* **39**, 1 (1989).
3. A. P. Ramirez, *J. Phys.: Condens. Matter* **9**, 39 (1997)
4. C. Felser, G. H. Fecher, and B. Balk, *Angewandte Chemie International Edition* **46**, 5 (2007).
5. H. Schmid, *Ferroelectrics* **162**, 1 (1994).
6. W. Eerenstein, N. D. Mathur, and J. F. Scott, *Nature* **442**, 7104 (2006).
7. R. Scherwitzl, P. Zubko, I. G. Lezama, S. Ono, A. F. Morpurgo, G. Catalan, and J. M. Triscone, *Adv. Mater.* **22**, 48 (2010).
8. A. Yu. Dobin *et. al.*, *Phys. Rev. B.* **68**, 11 (2003).
9. J. L. Garcia-Munoz, J. Rodriguez-Carvajal, P. Lacorre, and J. B. Torrance *Phys. Rev. B.* **46**, 8 (1992).
10. J. B. Torrance, P. Lacorre, A.I. Nazzal, E.J. Ansaldo, and Ch. Niedermayer, *Phys. Rev. B.* **45**, 14 (1992).
11. M . Medarde *et. al.*, *Phys. B (Amsterdam, Neth.)* **234-236** (1997).
12. R. Mallik, E. V. Sampathkumaran, J. A. Alonso, and M. J.Martinez-Lope, *J. Phys.: Condens. Matter* **10**, 18 (1998).
13. X. Granados, J. Fontcuberta, and X. Obradors, Ll. Manosa, and J. B. Torrance *Phys Rev. B.***48**, 16 (1993).
14. A. Tiwari, J. Narayan C. Jin, and A. Kvit, *Appl. Phys. Lett.* **80**, 8 (2002).
15. J. Blasco, M. Castro, and J. Garcia, *J. Phys.: Condens. Matter* **6**, 30 (1994).
16. J. E. Lorenzo, et. al, *Phys. Rev. B.* **71**, 4 (2005).
17. J. Liu, M. Kareev, B. Gray, J. W. Kim, P. Ryan, B. Dabrowski, J. W. Freeland, and J. Chakhalian, *Appl. Phys. Lett.* **96**, 23 (2010).
18. A. Venimadhav, I. Chaitanyalakshmi, and M.S. Hegde, *Mater. Res. Bull.* **37**, 2 (2002)
19. D. Kumar, K.P. Rajeev, J.A. Alonso, and M.J. Martinez-Lope, *J. Phys.: Condens. Matter* **21**, 48 (2009).
20. D. Kumar, K.P. Rajeev, J.A. Alonso, and M.J. Martinez-Lope, *J. Phys.: Condens. Matter* **21**, 18 (2009).